Available online at www.sciencedirect.com
SCIENCE DIRECT®
International Journal of Multiphase Flow 31 (2005) 239–252
International Journal of Multiphase Flow
www.elsevier.com/locate/ijmulflow

Brief communication

An experimental study on flow structures of a single bubble rising in a shear-thinning viscoelastic fluid with a new measurement technique

Tsao-Jen Lin *, Gen-Ming Lin

Department of Chemical Engineering, National Chung-Cheng University, Chia-Yi 621, Taiwan

Received 14 April 2004; received in revised form 13 October 2004

1. Introduction

There are many industrial processes which operate in the presence of gas bubbles with liquid as a continuous phase, such as fermentation, petrochemical, and other processing applications (Clift et al., 1978; Fan, 1989; Deckwer, 1992). It is recognized that the intrinsic dynamic behavior of bubble motion and associated wake interactions is the key factor responsible for mass and heat transfer (Grace et al., 1976; Bhaga and Weber, 1981; Fan and Tsuchiya, 1990). Nevertheless, numerous fluids used in industrial processes are non-Newtonian fluids, in which complex rheological properties result in a unique flow behavior different from that in Newtonian fluids (Barnett et al., 1966; Zana and Leal, 1978; Chhabra and DeKee, 1992; Chhabra, 1993). Although some studies have been conducted which unveil flow behavior involving bubble motion in non-Newtonian fluids, the fundamental understanding of their actions, especially in the quantitative aspect, is still inadequate.

Studying the flow characteristics of a single rising bubble provides the easiest start. It has been found that bubble shapes in Newtonian fluids are determined based on the balance of inertial, lift, viscous and surface tension forces (Clift et al., 1978; Rodrigue, 2002). Three important

* Corresponding author. Tel.: +886 5 2720411x33405; fax: +886 5 2721206.
E-mail address: chmtjl@ccu.edu.tw (T.-J. Lin).

0301-9322/$ - see front matter © 2004 Elsevier Ltd. All rights reserved.
doi:10.1016/j.ijmultiphaseflow.2004.11.004

dimensionless groups (i.e., Reynolds, Morton, and Eötvös) were proposed to constitute a map for the bubble shape regimes with Newtonian fluids (Bhaga and Weber, 1981). However, to date, no attempts have been successfully made to develop non-Newtonian versions of shape maps, because there is no sufficient rheological information available to construct a map similar to that for Newtonian fluids (Leal et al., 1971). According to the literature (Acharya et al., 1977; Dekee and Chhabra, 1988; Dekee et al., 1990; Leal et al., 1971), several investigators have performed visualization on the bubble shape transitions with increasing bubble size in different polymer concentrations. Although the physical rheological properties have crucial effects on the onset of bubble shape transition, bubbles generally display shape transitions from sphere, to prolate-teardrop, to oblate-cusped, to oblate spherical-cap, and to spherical cap with respect to bubble size.

The wake phenomena induced by a rising bubble in Newtonian fluids have been extensively studied for many years (Crabtree and Bridgwater, 1967; Bessler and Littman, 1987). By means of visualization, the averaged data or the qualitative description of wake properties, including shedding frequency, primary wake size, and bubble inclined angle, were determined (Tsuchiya and Fan, 1988). Three types of bubble wakes have been identified in Newtonian fluids, namely, the laminar wake, the transitional wake and the turbulent wake (Komasawa and Otake, 1980). Except for the laminar wake, wake shedding is always associated with other wake types. Through the utilization of advanced image acquisition and computer processing techniques, Chen and Chou (1998) and Chen et al. (1999) investigated the mechanism of alternative vortex shedding for a single air bubble rising in a water medium.

For non-Newtonian fluids, the bubble wake is very peculiar. Unlike the wake in the Newtonian fluids dragging the liquid with bubble moving upward, a negative wake in the non-Newtonian fluids is observed to push the liquid away from the bubble (Hassager, 1979). By laser-doppler anemometry (LDA), Bisgaard and Hassager (1982) concluded that a negative wake is induced by elasticity, which usually has the opposite-direction effect to the inertial force. With a particle image velocimetry (PIV) technique, Funfschilling and Li (2001) obtained a time averaged bubble flow field around bubbles rising in the polyacryamide (PAAm) solutions, and divided the bubble flow field into three different zones: a central down flow behind the bubble, a conical upward flow around the wake, and an upward flow zone in front of the bubble. From birefringence visualization, they qualitatively revealed a butterfly-like spatial distribution of the shear stresses around a bubble as well.

Although a lot of efforts have been made previously (Dziubinski et al., 2002), the instantaneous flow fields of a single bubble rising in non-Newtonian fluids have not been quantitatively investigated in the literature. Therefore, in this study, we provide the benchmark data for further computational modeling in order to resolve this insufficiency. In the past, the particle image analyzer (PIA) system has been adopted to study the flow structure of a single bubble rising in a two-dimensional bubble column. Through qualitative flow visualization, Chen et al. (1994) found that flow structures in 2-D and 3-dimensional (3-D) bubble columns are similar. Thus, in order to explore the complex macro- or micro-flow structure of bubble dynamics, we will examine two-dimensional behavior first. With the measured rheological properties, the important quantitative flow information of gas bubble dynamics in the non-Newtonian fluids can be analyzed. In addition, comparison of the differences of bubble wakes in the Newtonian and non-Newtonian media will be presented in this study.

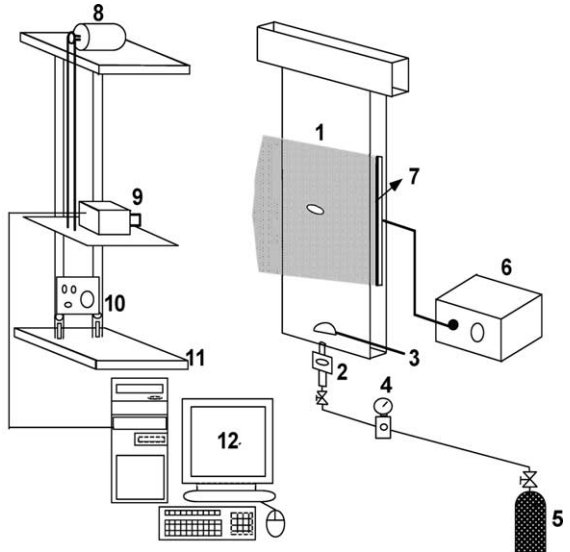

Fig. 1. Schematic diagram of the test facility.

2. Experimental setup

2.1. Flow facility and experimental conditions

The experimental apparatus is shown in Fig. 1. The apparatus includes a 2-dimensional column made of transparent Plexiglas sheets. This column is 30 cm in width, 1.2 cm in depth, and 120 cm in height. To study the mechanism of bubble rising, a hemispherical cup bubble injection is used to introduce a single bubble without pressure perturbation or any satellite generation. Air is used as gas phase. A specific volume of air metered by a needle valve was injected into a hemispherical cup. Bubble sizes up to 5 cm can be generated from the hemispherical cup bubble injector. In order to observe the flow structure in the near wake region, one needs to move at the same speed as the bubble. A bubble tracking system is constructed to carry a video camera and to move synchronously with the rising bubble. A DC motor powers this variable-speed tracking system. By adjusting the voltage of the DC motor, synchronous movements between the tracking system and bubble are accomplished.

The non-Newtonian fluid with a rheological shear-thinning property is the 1.5 wt% PAAm in demineralized water. Its rheological properties were measured by a RS1 (HAAKE) rheometer with a cylindrical spindle. Fig. 2 shows that the increasing shear rate causes a reduction in viscosity and an increase in the first normal stress difference (N_1). These results demonstrate that the PAAm solution is a shear-thinning and viscoelastic fluid. This shear-thinning behavior can be adequately described by an Ostwald–de Waele model (a power-law model) under steady shear:

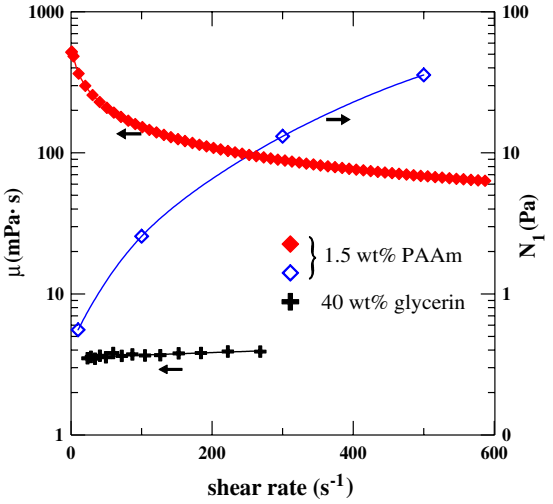

Fig. 2. Variations of viscosity and first normal stress difference (N_1) for the 1.5 wt% PAAm and 40 wt% glycerin solutions.

$$\tau_{yx} = m(\gamma_{yx})^n = \mu\gamma_{yx} \tag{1}$$

where $\mu = m(|\gamma_{yx}|)^{n-1}$. After algorithm regression, it is found that the value of the parameters m and n are 11.72 and 0.545, respectively. For comparison, a 40 wt% glycerin solution was applied as the Newtonian fluid. The viscosity of the glycerin solution shown in Fig. 2 is 3.76 mPa s. Neutrally buoyant polystyrene particles of 100 μm were used as liquid tracer particles. To ensure that the tracer particles followed the flow closely and had virtually no effects on the flow structure, the concentration of the seeding particles was maintained around 1% (v).

2.2. Experimental technique and interpolation data

The PIA system developed by Chen and Chou (1998) was applied to measure the instantaneous flow structure around a bubble rising in the 2-D bubble column. A light sheet 18 cm long generated from a straight light guide was projected from the sidewall to illuminate the tracers around the flow field. Connected with an optical fiber to the straight light guide, a 150 W halogen light source coupling with a special thermal filter lens provided a cold light to illuminate the flow field around the rising bubble. The image of the flow field was recorded by a high speed and high-resolution CCD camera, and then was stored in a computer for analysis. In this study, the recording rate was 500 s^{-1} for all the cases. Using a ruler along the flow field, the field of view for the Newtonian fluid was estimated to be 5×8 cm^2. For the Non-Newtonian fluid, the fields of view are 4.2×4.8 cm^2 for teardrop and oblate-cusped bubbles, and 7×7.8 cm^2 for oblate spherical-cap and spherical-cap bubbles, respectively.

The technique of PIA discriminates between tracer particles and bubbles based on the size of the recorded image of the objects. The vectors obtained were located at the position of the centroid of the initial tracer particle in a triplet. A commercial available program, TECPLOT, was utilized for post-processing the PIA data. For resolution of the analysis, a different grid number was used to

divide the field of view chosen to perform the interpolation for Newtonian and non-Newtonian cases, respectively. All of them resulted in a grid size of 2.0×2.0 mm^2. Execution of the interpolation process, using the Kriging algorithm, was performed for each phase frame. For the two-dimensional condition, the z-component vorticity $\omega_{xy}(i,j)$ and shear rate $\gamma_{xy}(i,j)$ of each grid point were calculated based on a finite-difference approximation for the interpolated velocity field. The shear stress in each grid point can be calculated by substituting $\gamma_{xy}(i,j)$ into the Ostwald–de Waele model.

The contours of vorticity and shear stress, for all shape bubbles, are nearly equivalent and approximately axisymmetric, which lead the flow structures to a stable pattern at all times. Although some insignificant values of vorticity, shear rate, and shear stress are not shown in the contour figures, this does not mean no value exists in the blank areas.

3. Results and discussion

In this study, instantaneous flow fields around a bubble rising in the 1.5 wt% PAAm and 40 wt% glycerin solutions have been induced to represent non-Newtonian and Newtonian fluids, respectively. Upon increasing the bubble size in the 1.5 wt% PAAm solution, the bubble shapes were transformed from prolate-teardrop, to oblate-cusped, to oblate spherical-cap, and to spherical-cap, while a circular-cap bubble in 40 wt% glycerin was induced to illustrate the mechanism of wake shedding. The test parameters of these bubbles are summarized in Table 1. According to Fig. 2, the viscosity of 1.5 wt% PAAm is about two orders of magnitude higher than that of 40 wt% glycerin. However, the rising velocity of the bubble size 2.7 cm in the 1.5 wt% PAAm is only slightly smaller than that of the bubble size 2.5 cm in 40 wt% glycerin. This can be attributed to the rheological effects on the flow structures for the non-Newtonian fluids, and will be discussed later.

Table 1
Test parameters of bubbles in Newtonian and non-Newtonian fluids

Bubble shape	Newtonian fluid (40 wt% glycerin)	Non-Newtonian fluid (1.5 wt% PAAm)			
	Circular-cap	Prolate-tear	Oblate-cusped	Oblate spherical-cap	Spherical-cap
Bubble breadth (D), cm	2.5	1.47	2.04	2.7	5.25
Bubble height (H), cm	1.0	1.41	1.36	1.25	1.8
Bubble thickness, cm	0.8	0.8	0.8	0.8	08
Equivalent diameter (d_e), cm	1.2	1.15	1.26	1.35	2.25
Bubble rise velocity (U_b), cm/s	21.443	15.34	17.15	20.15	36.46
Negative angle		70°	50°	Small	NA
Liquid density (ρ), g/cm^3	1.047	0.997			
Liquid viscosity (μ), g/cm s	3.76×10^{-2}				
Reynolds number	$Re = (U_b)D\rho/\mu$	$Re = (U_b)^{2-n}D^n\rho/m$			
	1492.7	5.57	7.84	11.55	39.33
Deborah number		$De = 2\lambda U_b/d_e$, $\lambda = 0.013$ s			
		0.347	0.354	0.388	0.421

3.1. Flow structure of a single bubble in the non-Newtonian fluid

3.1.1. Prolate-teardrop

Fig. 3 shows the analysis of the instantaneous flow structure for a prolate-teardrop bubble rising in a 1.5 wt% PAAm solution, including original image, and streamline, vorticity and shear rate contours. As the prolate-teardrop bubble rises upwards, the liquid in front of the bubble is suppressed and pushed away like a spring flow by the rising bubble, as shown in Fig. 3(b). Through calculating the difference of between two streamlines, we see that the suppressed flow contains a significant velocity gradient in front of the bubble. An example in Fig. 4 can confirm the existence of the high radial and axial velocity gradients by simply examining the slopes and the difference of two radial distributions ($y/H = 1.25$ and 1.5) of the vertical liquid velocity. After integrating the shear rate into a contour, Fig. 3(d) shows that two high shear-rate zones are individually located at two front sides of the bubble which transfer the momentum away from the bubble. Due to the shear-thinning effect, the viscosity of the suppressed liquid has been reduced. The drag force exerted on the bubble is reduced, and the bubble rise velocity is consequently increased. However, there is no significant vorticity generated in the suppressed flow in spite of the deformed flow structure, as shown in Fig. 3(c).

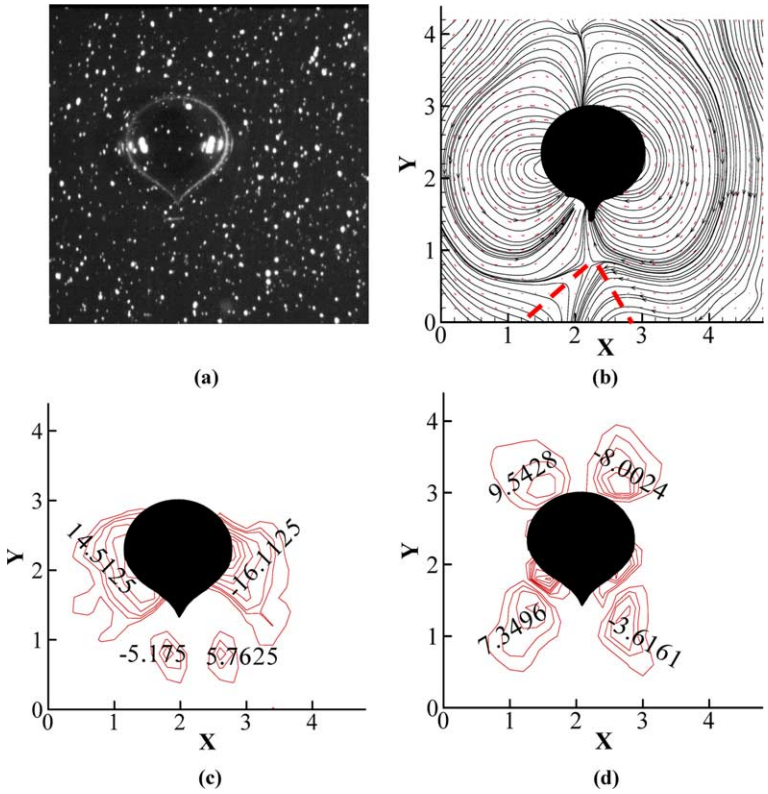

Fig. 3. (a) Original image, (b) streamline, (c) vorticity, and (d) shear rate contours of a prolate-teardrop bubble rising in a 1.5 wt% PAAm solution.

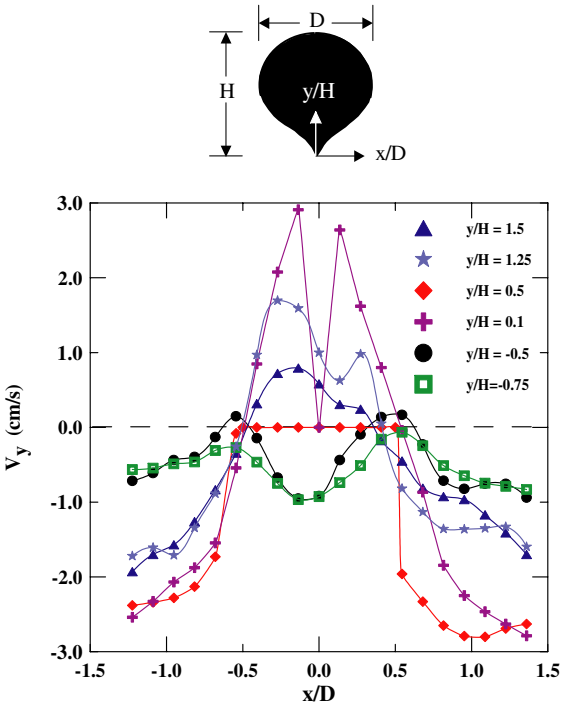

Fig. 4. Radial distribution of the vertical liquid velocity at various locations around the prolate-teardrop bubble rising in a 1.5 wt% PAAm solution.

Moreover, Fig. 3(b) shows that the suppressed flow alters its direction downward, and then circulates to the rear of the bubble. This phenomenon of circulation might be attributed to two factors: (i) the negative pressure induced by the wake existing behind the bubble, and (ii) the viscoelastic effect of the fluid causing the fluid to recoil back to its original status. From Table 1, the Deborah number for this bubble is estimated to be around 0.347, which means that the deformed fluid elements are not fully recoiled and still have some viscoelastic effects remaining immediately after the passage of the bubble. The existence of a higher vorticity zone at both sides of the bubble, as shown in Fig. 3(c), can also be evidence to illustrate the viscoelastic effect. These vorticities provide an angular momentum to alter the direction of the flow, like a circulated flow. However, it is hard to say which factor was more important for causing this circulation. The discovered relation between the suppressed and circulated flows seems different from that reported by Funfschilling and Li (2001), in which they observed that the conical upward flow (i.e., the circulated flow) beneath the bubble is independent of the upward flow zone (i.e., the suppressed flow) in front of the bubble. The discovery of this dissimilarity resulted from the different observation coordinates: the Euler system for Funfschilling and Li, but the Lagrange system for this study.

Further examining Fig. 3(b), we see the inner parts of the circulated flows from both sides of the flow to the rear of the bubble continuously deform the bubble shape inwards. In the end, a cusped shape is formed at the tail of the bubble due to distortion and compression from the circulated flow. From Fig. 4, the circulated flow ($y/H = 0.1$) shows a large vertical liquid velocity and a high

velocity gradient at both sides of the cusp, which supply the momentum to deform the bubble. Due to transferring this momentum, two high shear-rate zones individually exist at both sides of the cusp as shown in Fig. 3(d). On the other hand, the rest of the circulated flows come across from both sides, merge, and turn to a downward flow tangentially. The zone of these downward flows is the so-called negative wake. The turning points of the downward flows are the boundary of the negative wake, which exhibits a conical shape as indicated in Fig. 3(b). From the recorded images, the angle of the conical negative wake is about 70°. Two opposite vorticities are generated on the conical boundary of the negative wake to supply the altering energy for the flow, as shown in Fig. 3(c). Unlike the shedding wake in Newtonian fluids which drag the bubble, the negative wake provides a positive effect on bubble rise due to its departing from the bubble. Therefore, the negative wake is the second mechanism to promote bubble rise velocity in non-Newtonian fluids.

The shear stress distribution around a teardrop bubble is shown in Fig. 5(a). From this figure, we see that two pairs of axisymmetric stresses exist around the rising bubble: one pair is in front of the bubble and the other is in the circulated upward flow and at the interface of the negative wake behind the bubble. No significant shear stress is found in the negative wake because of the small velocity gradient in the downward flow. From the radial distributions at $y/H = -0.5$ and -0.75, an approximately flat velocity distribution in the negative wake area verifies the above statement, as shown in Fig. 4. Additionally, the shear stress contour matches very well with the image of the birefringence visualization measured by Li et al. (1998), as shown in Fig. 5. This is the first time shear stress distribution as reported has been directly calculated from flow field and rheological properties.

3.1.2. Other bubbles

Fig. 6 shows the images and analyses for the other three bubbles, including oblate-cusped, oblate spherical-cap, and spherical cap bubbles. Note that the larger the bubble size, the greater the

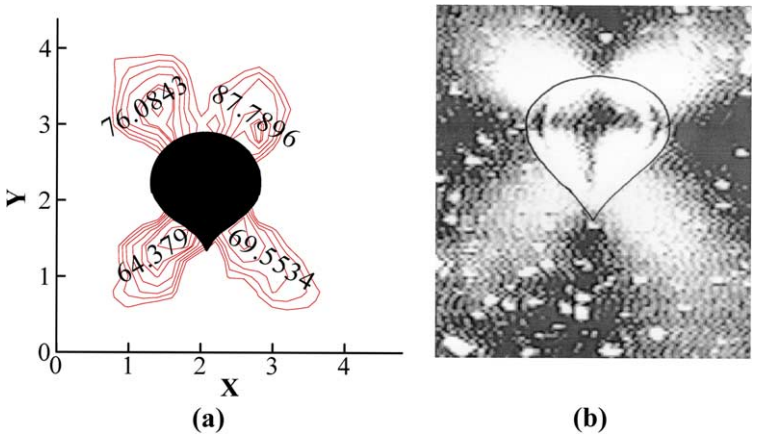

Fig. 5. Comparison of (a) the shear stress contour of a prolate-teardrop bubble rising in a 1.5 wt% PAAm solution and (b) the image of birefringence visualization (after Li et al., 1998).

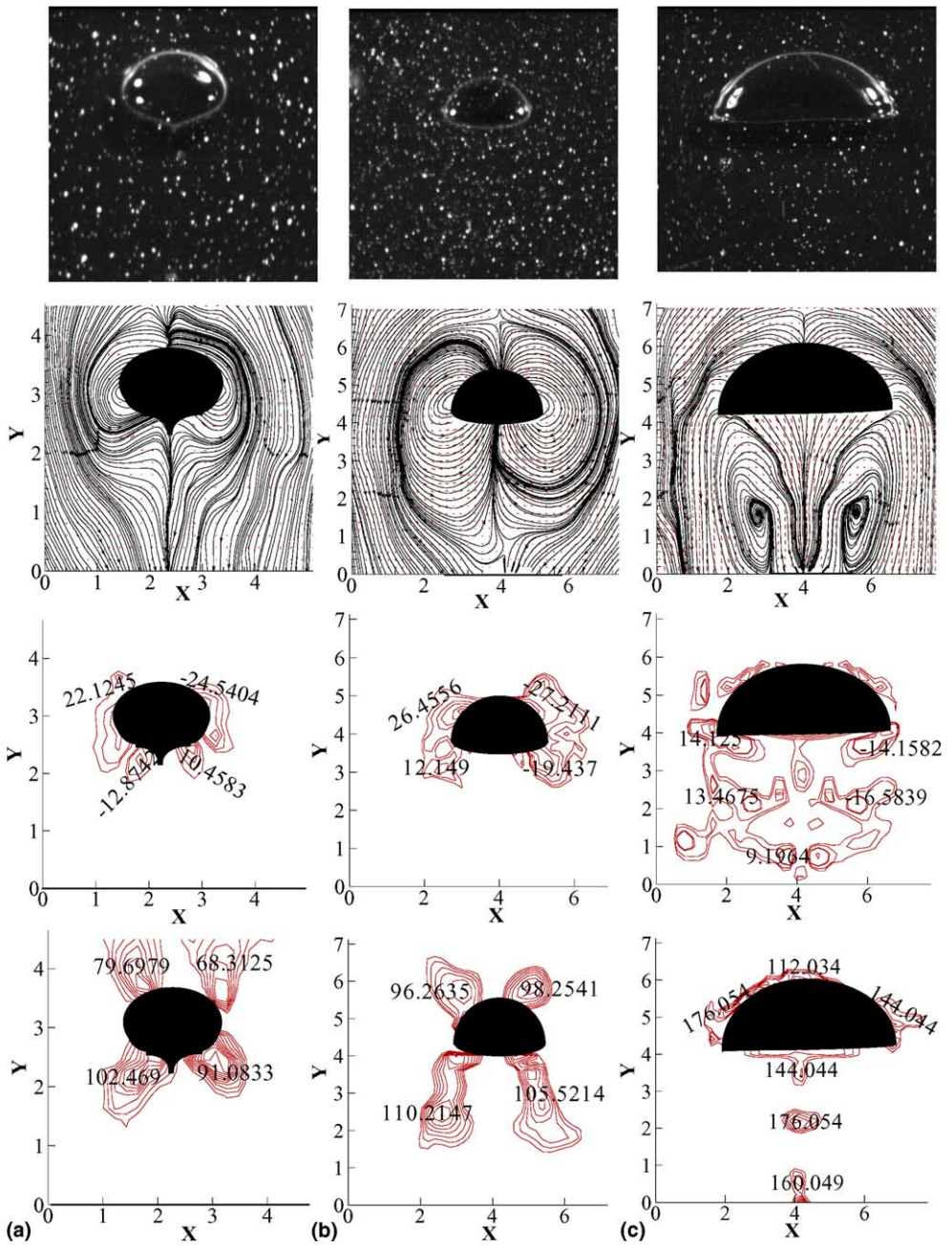

Fig. 6. Original image, streamline, vorticity, and shear stress contours of the (a) oblate-cusped, (b) oblate spherical-cap, and (c) spherical-cap bubble rising in a 1.5 wt% PAAm solution.

gas momentum to suppress the liquid in front of the bubble. Except for the spherical cap bubble, the strengths of the pairs of the axisymmetric shear stresses and vorticities consequently become larger as they increase with bubble size. By comparison, it is found that the angle of negative wake

gradually shrinks with increasing bubble size, and finally ceases to exist in the spherical-cap bubble. Due to this evolution of negative wake with increasing bubble size, the cusp vanished from the shape of the oblate spherical-cap and spherical-cap bubbles. This phenomenon might be attributed to an increase in bubble size; an induced higher shear rate can enhance the viscoelastic effect to prolong the flow recoiling. The increase of the Deborah number with bubble size can be another reason for this explanation. Hence, for the oblate spherical-cap bubble, the suppressed flow almost circulates to the rear of the bubble and only a little liquid turns to downward flow, as shown in Fig. 6(b). The zone of the negative wake becomes very narrow for the oblate spherical-cap bubble.

For the spherical-cap bubble, instead of a negative wake, a pair of closed vortices steadily exists behind the bubble and exchanges no liquid with the external flow, as shown in Fig. 6(c). This figure reveals that the suppressed flow does not suck back to the bubble, just encapsulating this pair of vortices at the outside. This pair of vortices looks like a closed laminar wake, which is usually observed behind a circular-cap bubble rising in a Newtonian fluid. From Table 1, the Reynolds number of the spherical-cap bubble is relatively small ($Re = 39.33$) and in the laminar region. In principle, there should be no vortex formed in the bubble wake under this flow region. Accord-

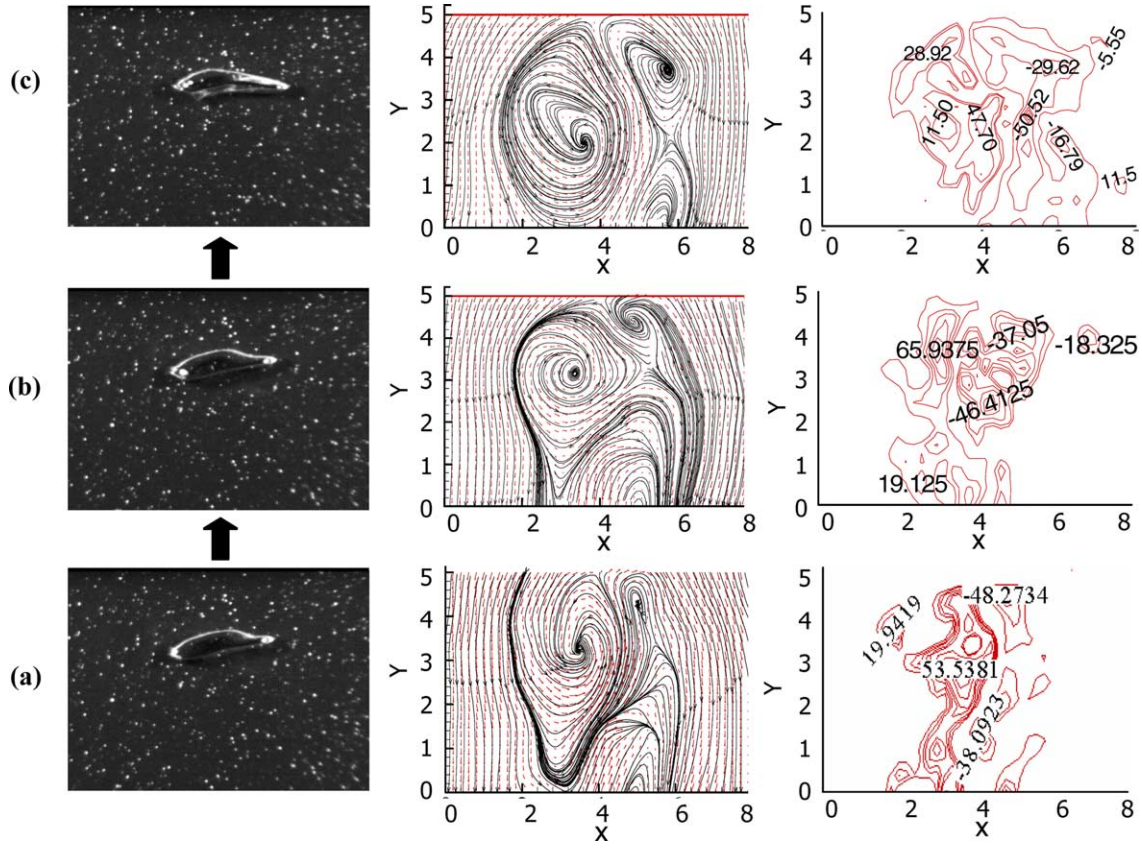

Fig. 7. Original image, streamline, and vorticity contours for six consecutive instantaneous wake sheddings of the Newtonian fluid.

ing to the instability theory, this result might be explained by postulating that during fluid recoiling, some small turbulent eddies were induced in the circulated flow, augmented together, and as a result overcame the inertial force to become a pair of large vortices. This is the reason why a lot of vorticities exist at the boundary of the vortex to supply the energy for the formation of the vortex. Of course, the negative pressure behind the spherical-cap bubble is another essential driving force for the formation of the vortex. It is surprising that no significant shear stress remained with in the vortices, but instead in between the vortices after the integrating calculation. This might indicate that the fluid within the vortices has almost recoiled and only the fluid in between the vortices is repressed and sheared by the rotating vortices to induce the shear stress. Moreover, a thin layer of shear stress is observed, located at the frontier of the bubble. Because of the resolution of the image, only limited data was used to analyze the flow behavior in front of the bubble. No conclusion at this moment has been made on whether or not there are two shear stress zones in front of the bubble. Likewise, the reason for the location of the stress zones behind the vortices has not been postulated. Further study on this spherical-cap bubble is needed.

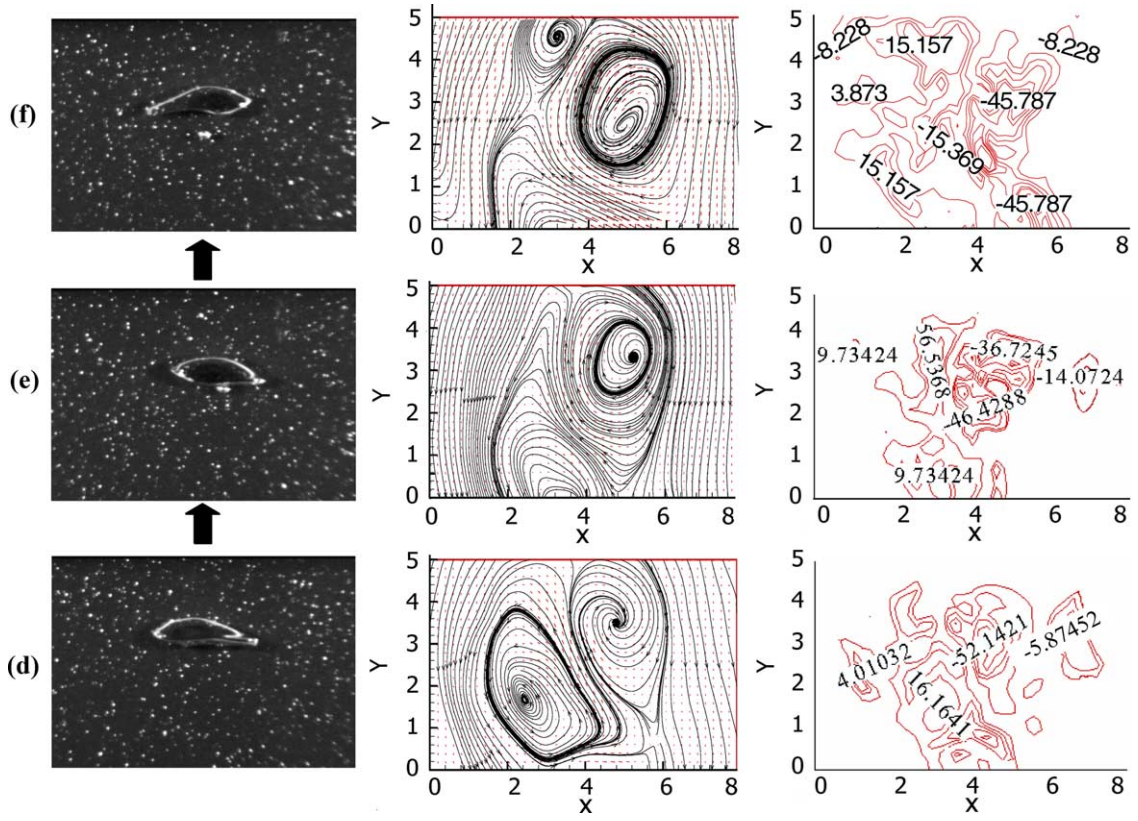

Fig. 7 (*continued*)

3.2. Bubble wakes in newtonian fluids

A detailed discussion regarding the mechanisms of wake shedding in Newtonian fluids has been published in several papers (e.g., Chen and Chou, 1998; Chen et al., 1999). Here, an example of the flow structures in a Newtonian fluid is used for comparing and enlightening the difference in the non-Newtonian fluid. Because a wobbling movement is induced during a bubble rises through a Newtonian fluid, the flow patterns indeed are more complicated than those in a non-Newtonian fluid. In order to simplify the measurement in the Newtonian fluid, only the bubble wake region right behind the bubble was used for the analysis. The original images, integrated streamlines, and vorticity contours for the time-series of the half-cycle of the wake-shedding process are given in Fig. 7. As a bubble rises, a descending free stream from the suppressed flow is located outside the boundary of its wake. It is found that a velocity difference exists inbetween the wake and the free stream. Due to Kelvin–Helmholtz instability, small-scale vorticities are continuously generated from both sides of the free shear layer to the wake. Small-scale vorticities can be either dispersed to generate turbulent stresses, or eventually accumulated to form a large-scale vortex (Strouhal vortex). Formation of a large-scale vortex can be verified by the merger of the right-hand-side vortex as shown in Fig. 7(b)–(e). The unequal balance of dissipation and diffusion of small-scale vorticities entrains the free stream to cut through one side of the wake boundary. This procedure results in vortex shedding, as one can see in the detachment of the left-hand-side vortex in Fig. 7(c)–(f). Hence, this mechanism is the so-called bubble wake shedding that we see in Newtonian fluids, which is totally different from that of the negative wake in the non-Newtonian fluid. Shear-thinning and viscoelastic properties of the non-Newtonian fluid are the two main factors for the difference in wake structures.

4. Conclusion

The instantaneous flow structure and other hydrodynamic information of four single bubbles rising in a Non-Newtonian fluid have been quantitatively studied through a measurement technique combining the PIA and rheological data. The liquid in front of the bubble was suppressed and circulates back to the bubble due to the effects of non-Newtonian properties: shear-thinning and viscoelasticity. Except for the spherical-cap bubble, two pairs of high shear stress zones are individually formed in the front and the rear of the bubble, matching the results of birefringence very well. Besides, the existence of the pair of vorticity zones is evidence of energy supply for circulating the suppressed flow to the rear of the bubble. The contours of vorticity and shear stress are nearly equivalent and axisymmetric, which leave the flow structures of the bubble stable on its ascent. The formation mechanism of negative wake from part of the circulated flow is different from the results proposed by Funfschilling and Li (2001). With increasing bubble size, the angle of the conical negative wake gradually shrinks, and finally disappears at the spherical-cap bubble. Concerning the spherical-cap bubble, instead of the negative wake, a pair of closed vortices steadily exists behind the bubble due to the instability of turbulent eddies. Shear stresses are found only in between the pair of vortices and at the frontier of the spherical-cap bubble. The wake shedding in the Newtonian fluid was induced through unequal balance of small-scale vorticities to entrain the free stream, thereby cutting through one side of the wake boundary and shedding the

vortex. The mechanism of wake shedding in the Newtonian fluid is thus different from that of the negative wake in the non-Newtonian fluid.

Acknowledgments

This work was supported by the National Science Council grant 92-2214-E-194-007 in The Republic of China.

References

Acharya, A., Mashelkar, R.A., Ulbrecht, J., 1977. Mechanics of bubble motion and deformation in non-Newtonian media. Chem. Eng. Sci. 32, 863–872.

Barnett, S.M., Humphrey, A.E., Litt, M., 1966. Bubble motion and mass transfer in non-Newtonian fluids. AIChE J. 12, 253–256.

Bessler, W.F., Littman, H., 1987. Experimental studies of wake behind circularly capped bubbles. J. Fluid Mech. 185, 137–151.

Bhaga, D., Weber, M.E., 1981. Bubbles in viscous liquids: shapes, wakes and velocities. J. Fluid Mech. 105, 61–85.

Bisgaard, C., Hassager, O., 1982. An experimental investigation of velocity fields around spheres and bubbles moving in non-Newtonian liquid. Rheol. Acta 21, 537–548.

Chen, R.C., Chou, I.S., 1998. Wake structure of a single bubble rising in a two-dimensional column. Expt. Therm. Fluid Sci. 17, 165–178.

Chen, R.C., Reese, J., Fan, L.-S., 1994. Flow structures in a three-dimensional bubble column and three-phase fluidized bed. AIChE J. 40, 1093–1104.

Chen, R.C., Wang, F.M., Lin, T.-J., 1999. Bubble wake dynamics of a single bubble rising in a two-dimensional liquid–solid fluidized bed. Chem. Eng. Sci. 54, 4831–4838.

Chhabra, R.P., 1993. Bubbles, Drops, and Particles in non-Newtonian Fluids. CRC Press, Boca Raton, Florida.

Chhabra, R.P., DeKee, D., 1992. Fluid Particles in Rheologically Complex Media, in Transport Processes in Bubbles, Drops and Particles. Hemisphere, New York.

Clift, R., Grace, J.R., Weber, M.E., 1978. Bubbles, Drops and Particles. Academic Press, New York.

Crabtree, J.R., Bridgwater, J., 1967. The wakes behind two-dimensional air bubbles. Chem. Eng. Sci. 22, 1517–1522.

Deckwer, W.-D., 1992. Bubble Column Reactors. John Wiley and Sons, New York.

Dekee, D., Chhabra, R.P., 1988. A photographic study of shapes of bubbles and coalescence in non-Newtonian polymer solutions. Rheol. Acta 27, 372–656.

Dekee, D., Chhabra, R.P., Dajan, A., 1990. Motion and coalescence of gas bubbles in non-Newtonian polymer solutions. J. Non-Newtonian Fluid Mech. 37, 1–18.

Dziubinski, M., Orczykowska, M., Budzynski, P., 2002. Srednia wartosc naprezenia stycznego i szybkosci scinania na powierzchni pecherza gazowego przeplywajacego w cieczach nieNewtonowskich (Average value of shear stress and shear rate at the surface of gas bubble rising in non-Newtonian liquids). Inzynieria Chemiczna i Procesowa 23, 341–348.

Fan, L.-S., 1989. Gas–Liquid–Solid Fluidization Engineering. Butterworth-Heinenann, Stoneham, MA.

Fan, L.-S., Tsuchiya, K., 1990. Bubble Dynamics in Liquids and Liquid–Solid Suspension. Butterworth-Heinenann, Stoneham, MA.

Funfschilling, D., Li, H.Z., 2001. Flow of non-Newtonian fluids around bubbles: PIV measurements and birefringence visualization. Chem. Eng. Sci. 56, 1137–1141.

Grace, J.R., Wairegi, T., Nguyen, T.H., 1976. Shapes and velocities of single drops and bubbles moving freely through immiscible liquids. Trans. Inst. Chem. Eng. 54, 167–173.

Hassager, O., 1979. Negative wake behind bubbles in non-Newtonian liquids. Nature 279, 402.

Komasawa, I., Otake, I., 1980. Wake behind and its effect on interaction between spherical-cap bubble. J. Chem. Eng. Jpn. 13, 103–109.

Leal, L.G., Skoog, J., Acrivos, A., 1971. On the motion of gas bubbles in a viscoelastic liquid. Can. J. Chem. Eng. 49, 569–578.

Li, H.Z., Mouline, Y., Funfschiling, D., Marchal, P., Choplin, L., Midoux, N., 1998. Evidence for in-line bubble interactions in non-Newtonian fluids. Chem. Eng. Sci. 53, 2219–2230.

Rodrigue, D., 2002. A simple correlation for gas bubbles rising in power-law fluids. Can. J. Chem. Eng. 80, 289–292.

Tsuchiya, K., Fan, L.-S., 1988. Near-wake structure of a single gas bubble in a two-dimensional liquid-solid fluidized bed: vortex shedding and wake size variation. Chem. Eng. Sci. 43, 1167–1181.

Zana, E., Leal, L.G., 1978. Dynamics and dissolution of gas bubbles in a viscoelastic fluid. Int. J. Multiphase flow 4, 237–262.